Crime Modeling with Truncated Lévy Flights and Effects of Police Patrol

Chaohao Pan[†], Bo Li[∗], Yuqi Zhang[†], Nathan Geldner[∗],
Chuntian Wang[†], Li Wang[†], Andrea Bertozzi[†]

January 15, 2016

Abstract

In this paper, we developed a truncated Lévy flight model to study the crime dynamics. In the discrete case, our model allows criminals to perform long jumps in between committing crimes with a speed light. This is a more realistic extension of a pioneering random walk model by Short et. al [M. Short, et al., *Math. Models Methods Appl. Sci., 18 (2008)*, pp. 1249-1267] and a Lévy flight model thereafter in [S. Chaturapruek, et al., *SIAM J. Appl. Math., 73(4) (2013)*, pp. 1703–1720]. We also derive a continuum limit and perform a stability analysis to study the formation of crime hotspots. Our model is more realistic than the Lévy Flight Model, and provides an alternative to the Random Walk Model when the criminals can perform long jumps in between committing crimes. In the next step, we introduce patrolling police officers to our new model following that in [P. Jones, et al., *Math. Models Methods Appl. Sci., 20 (2010)*, pp. 1397-1423]. We examine the effects of police patrol when the police choose to adopt different strategies, including unbiased random walk, biased random walk, and truncated Lévy flight. We evaluate the effectiveness of the police patrol with the number of crime events in a given time frame. With spatially non-uniform initial conditions, we find that the truncated Lévy flight to be the best strategy in general.

Keywords: Crime models; Lévy flight; continuum limit; linear stability; police patrol.

2010 *Mathematics Subject Classification* Primary: 35R60; Secondary: 35Q84.

[∗]Department of Mathematics, Harvey Mudd College, Claremont, CA 91711
[†]Department of Mathematics, University of California, Los Angeles, Los Angeles, CA 90095

Contents

1   Introduction

Crime modeling is a growing field of mathematical modeling. Notable contributions can be attributed to the UCLA models [19, 1], which has helped thirty cities worldwide curb crime. This model, hereafter referred to as the "Random Walk Model (RWM)", assumes that the criminals follow a random walk that is biased toward regions with high "attractiveness". The concept of "attractiveness" is rooted in criminology research. When a crime happens at a given place, that place as well as places nearby become more attractive to similar crimes [19, 3, 22]. This phenomenon is known as the repeat or near-repeat victimization, which depends on whether a criminal revisit the previous place or a neighboring place respectively. Some have likened this phenomenon to the "broken windows effect" whereby disorder and minor crimes such as jaywalking and littering lead to an increase in major crimes like burglary and murder. In previous crime models, the broken windows effect is usually treated together with repeat and near-repeat victimization as a critical factor determining the change in attractiveness [9, 6, 3, 22]. The Random Walk Model successfully picks up the crime hotspots: i.e., disjoint areas with high crime rates [20, 8]; and compares favorably with the real data [18].

However, the assumption that criminals take a random walk with constant velocity is a very restricted one. In real life, criminals can take a train or other vehicle and move much farther than a similar criminal on foot. Previous researches have shown that human motions are better modeled with Lévy flights, instead of random walks [10, 2, 7]. Also, data of distances between homes of criminals and their targets suggests that they are willing to make long trips for valuable targets [17, 21]. To this end, Chaturapruek et al. developed a new model by assuming that the criminals undergoes a Lévy flight in [4], i.e., criminals can go anywhere in one time step with a probability proportional to attractiveness and inversely proportional to some power μ of distance [5]. We refer this model as the "Lévy Flight Model (LFM)" from now on.

Nevertheless, a real criminal can only move as fast as traffic or public transit, i.e., the property of LFM that criminals can take arbitrarily long jumps in a time step does not accurately reflect the reality. Furthermore, movement patterns of different types of criminals can vary greatly. As was shown in [21, 12], professionals and older criminals can travel faster than amateur and younger criminals. With these facts in mind, we propose a Truncated Lévy Flight Model (TLFM) for the movement of criminals, in which we eliminate arbitrarily long jumps by imposing a speed limit on the Lévy flight. Truncated Lévy flights have been applied in the field of finance [15, 13, 16], and it is proven that the sum of independent truncated Lévy flights converges to a Gaussian process [14]. In the continuum limit, our model involves only a Laplace operator, which differs from that of the Random Walk Model only by a scaling constant. This is because our model incorporates both the "nonlocal" feature of criminals by allowing them long range jumps and the "local" feature of them that is restricted by the speed limit. Additionally, with varying speed limits, TLFM can simulate criminals' movement patterns of different types. For example, to simulate dynamics of amateur or younger criminals, we take the speed limit to be small, which leads to a pattern that is similar to that generated by RMW. Likewise, if there is a group of professional criminals with better mobility, we can increase the speed limit accordingly. In this case, the generated pattern will look like the pattern generated by LFM, except that the unrealistic long jumps will no longer occur. We also show that, quantitatively, both RWM and LFM are special cases of TLFM. Another remarkable feature of TLFM is that the Laplace operator in the continuum system, other than the fractional Laplace operator

3

in the Lévy Flight Model [4, 24], is more amenable to various kinds of boundary conditions numerically.

In the next step, we examine the effects of police patrol on TLFM as following. We adopt a basic assumption in [11] that the attractiveness of a site decreases exponentially with the number of police officers at that site. There, based on RWM, three executable strategies are designed for the police officers: an unbiased random walk, a random walk biased towards the sites with high attractiveness, and a "peripheral interdiction" which send police officers to perimeters (instead of the center) of crime hotspots. However, since the criminals in TLFM can take long jumps, protecting the perimeters of a hotspot does not necessarily prevent criminals from entering the center of the hotspot. As a result, we do not consider "peripheral interdiction" in this paper. Instead, we also let the police officers do a truncated Lévy flight biased towards the hotspots as a patrol strategy. By measuring the total number of crimes committed, we compare the effects of police adopting different strategies: an unbiased random walk, a biased random walk, and a biased truncated Lévy flight. With experiments on different initial conditions, we found that the biased truncated Lévy flight is the best strategy for the police in general.

The rest of paper is organized as follows. In Section 2, we review the basic assumption of the repeat and near-repeat victimization, and then derive, in both discrete and continuum settings, the biased truncated Lévy flight for the criminals. For the continuum system, we perform a linear stability analysis on the homogeneous steady state solution to study the formation of hotspots. We also explore the relations between TLFM with previous RWM and LFM. Then in Section 3, we incorporate the effects of law enforcement. By comparing the efficiency of different patrol strategies, we see that the biased truncated Lévy flight is the best strategy in general. We also simulate the police patrol in a two dimensional domain, and obtain the same conclusion. Finally, an appendix for details of derivations and proofs in Section 2.5.

2 Modeling Criminal Behaviors with the Truncated Lévy Flight

In this section, we will describe the model in which there are only criminals but no police. These models can be defined on any connected graph (which accurately reflects the geometry of a city). As a first step, we define the models on a one-dimensional grid graph with grid length l with periodic boundary conditions, unless otherwise specified. We will define first the dynamics of the local attractiveness and then the evolution of the distribution of the criminals.

2.1 Local Attractiveness

As in [19, 4, 11], we define the varying vulnerability to burglary events of different sites as follows. For each burglary site k, we define a dynamic attractiveness. Criminals are more likely to travel to more attractive areas, and more likely to commit crimes once there. To describe the evolution of attractiveness over time, we decompose the attractiveness field as

$$\mathbf{A}_k(t) = A_k^0 + \mathbf{B}_k(t), \tag{1}$$

where A_k^0 is a static term depending only on k, and $\mathbf{B}_k(t)$ is a dynamic term related to the effects of repeat and near-repeat victimization.

4

Now we take into account the repeat and near-repeat victimization. We define $\mathbf{E}_k(t)$ to be the number of crimes committed in the time interval $(t, t + \delta t)$ at site k. Considering the self-exciting nature of crime, and temporarily neglecting the near-repeat victimization effect, we can then express the evolution of $\mathbf{B}_k(t)$ as $\mathbf{B}_k(t + \delta t) = \mathbf{B}_k(t)(1 - \omega\delta t) + \theta\mathbf{E}_k(t)$, where ω is the decay rate of the attractiveness field, and θ is the increase in $\mathbf{B}_k$ for each crime that occurs at k. If we also consider the near-repeat victimization, the evolution equation of $\mathbf{B}_k(t)$ can be expressed as

$$\mathbf{B}_k(t + \delta t) = \left[(1 - \eta)\mathbf{B}_k(t) + \frac{\eta}{2}(\mathbf{B}_{k-1}(t) + \mathbf{B}_{k+1}(t))\right](1 - \omega\delta t) + \theta\mathbf{E}_k(t), \qquad (2)$$

where $\eta \in (0, 1)$ is a constant measuring the significance of the near-repeat victimization effect.

Initially, a given number of criminals are distributed over the graph. The movement of criminals is restricted to discrete time steps $t = n\delta t, n \in \mathbb{N}$. We define $\rho_k(t)$ to be the average number of criminals at site k during the time interval $[t, t + \delta t)$. At each time step, a criminal either moves to another burglary site or commits a crime. We consider a criminal committing a crime in the time interval $(t, t + \delta t)$ at site k as a standard Poisson process, the probability of which, $p_k(t)$, is given by

$$p_k(t) = 1 - e^{-A_k(t)\delta t}, \qquad (3)$$

where $A_k(t)$ denotes the expectation of $\mathbf{A}_k(t)$. We also denote the expectation of $\mathbf{B}_k(t)$ as $B_k(t)$. Then it follows immediately from (1) that

$$A_k(t) = A_k^0 + B_k(t). \qquad (4)$$

Moreover, in accordance with a standard Poisson process, the expectation of $\mathbf{E}_k(t)$ is $\delta t A_k(t)\rho_k(t)$ Thus we take the expectation of both sides in (2), and obtain

$$B_k(t + \delta t) = \left[(1 - \eta)B_k(t) + \frac{\eta}{2}(B_{k-1}(t) + B_{k+1}(t))\right](1 - \omega\delta t) + \theta\delta t A_k(t)\rho_k(t). \qquad (5)$$

2.2 The Discrete Truncated Lévy Flight

In the Random Walk Model, the criminals can only move to a neighboring site in each time step. By contrast, in the Lévy Flight Model, we allow the criminals to move to any site on the graph. As in [4], we define the relative transition likelihood $w_{i \to k}$ subject to the following Lévy power law

$$w_{i \to k} = \frac{A_k}{(l|i - k|)^\mu}, \qquad (6)$$

where $\mu \in (1, 3)$. In other words, although arbitrarily long jumps are allowed in a Lévy flight, the probability of traveling to a distant site in one time step is low.

Moreover, in contrast with the Lévy Flight Model, for the truncated Lévy flight, one can move no more than L gridspaces within one time step, with $L \in \mathbb{Z}, L \geq 1$. The relative transition likelihood, still denoted as $w_{i \to k}$ with abuse of notation, is defined as follows

$$w_{i \to k} = \begin{cases} \frac{A_k}{l^\mu|i-k|^\mu}, & 1 \leq |i - k| \leq L, \\ 0 & \text{otherwise.} \end{cases} \qquad (7)$$

The (normalized) transition probability is then defined as

$$q_{i \to k} = \frac{w_{i \to k}}{\sum_{j \neq i} w_{i \to j}}.$$ (8)

Following the settings in the Random Walk Model as in [19], the criminals obey the following rules: in the time interval $(t, t + \delta t)$, a criminal either commits a crime which obeys the standard Poisson process or else moves on according to a biased truncated Lévy flight; also, some new criminals appear with a constant rate Γ. Given the criminal density at time t, the criminal density after one time step can be calculated as

$$\rho_k(t + \delta t) = \sum_{\substack{i \in \mathbb{Z} \\ 1 \leq |i-k| \leq L}} [1 - A_i(t)\delta t]\rho_i(t)q_{i \to k}(t) + \Gamma \delta t.$$ (9)

2.3 The Continuum Limit of TLFM

Now we take the continuum limit for the above discrete model as δt and l both converge to 0. Firstly we observe that, following the same procedure as in [4], we can derive the continuum limit for (5) as follows

$$A_t = \frac{l^2 \eta}{2\delta t} A_{xx} - \omega(A - A_0) + A\rho\theta,$$ (10)

where we write $\frac{\partial A}{\partial t}$ as A_t for consistency of notation. We will use the same type of notations for partial derivatives hereafter.

The derivation of the continuum limit for ρ, however, is more difficult, and much different from the process in [4] due to the truncation.

First, we define

$$z_L := 2\sum_{k=1}^{L} \frac{1}{k^\mu},$$ (11)

and

$$\mathcal{L}(f_i) := \sum_{\substack{j \in \mathbb{Z} \\ 1 \leq |i-j| \leq L}} \frac{f_j - f_i}{(|j-i|l)^\mu}.$$ (12)

Then it follows immediately from (7) that

$$\sum_{\substack{i \in \mathbb{Z} \\ 1 \leq |i-k| \leq L}} w_{i \to k} = l^{-\mu} z_L A_i + \mathcal{L}(A_i).$$ (13)

With (13) and (8), we obtain

$$\begin{aligned}
q_{i \to k} &= \frac{w_{i \to k}}{\sum_{\substack{j \in \mathbb{Z} \\ 1 \leq |j-k| \leq L}} w_{i \to j}} = \frac{w_{i \to k}}{l^{-\mu} z_L A_i \left(\frac{\mathcal{L}(A_i)}{l^{-\mu} z_L A_i} + 1 \right)} \\
&\sim w_{i \to k} \left[\frac{1}{l^{-\mu} z_L A_i} - \frac{\mathcal{L}(A_i)}{(l^{-\mu} z_L A_i)^2} \right] \\
&= \frac{A_k}{|i-k|^\mu} \left(\frac{1}{z_L A_i} - \frac{\mathcal{L}(A_i) l^\mu}{A_i^2 z_L^2} \right), \quad 1 \leq |i-k| \leq L,
\end{aligned}$$ (14)

6

where, in the second step, we have applied the approximation $\frac{1}{1+x} \sim 1 - x$ for small x. We then obtain by (9)

$$\frac{\rho_k(t + \delta t) - \rho_k(t)}{\delta t} = \frac{1}{\delta t}\left[\sum_{1 \le |i-k| \le L} \rho_i(1 - A_i\delta t)q_{i \to k} - \rho_k\right] + \Gamma. \tag{15}$$

Now applying (14) to the RHS of (15), we obtain

$$\begin{aligned}
\frac{\rho_k(t + \delta t) - \rho_k(t)}{\delta t} &= \frac{1}{\delta t}\sum_{1 \le |i-k| \le L} \rho_i(1 - A_i\delta t)\frac{A_k}{|i-k|^\mu}\left(\frac{1}{z_L A_i} - \frac{\mathcal{L}(A_i)l^\mu}{A_i^2 z_L^2}\right) - \frac{\rho_k}{\delta t} + \Gamma \\
&= \frac{A_k}{\delta t}\left[\sum_{1 \le |i-k| \le L}(1 - A_i\delta t)\frac{\rho_i}{A_i}\frac{1}{z_L|i-k|^\mu} - \frac{\rho_k}{A_k}\right] \\
&\quad - \frac{A_k}{\delta t}\sum_{1 \le |i-k| \le L}\left[(1 - A_i\delta t)\frac{\rho_i}{|i-k|^\mu}\frac{\mathcal{L}(A_i)l^\mu}{A_i^2 z_L^2}\right] + \Gamma.
\end{aligned} \tag{16}$$

We also find that (11) and (12) implies

$$\sum_{\substack{i \in \mathbb{Z} \\ 1 \le |i-k| \le L}}\frac{\rho_i}{|i-k|^\mu} = \sum_{\substack{i \in \mathbb{Z} \\ 1 \le |i-k| \le L}}\frac{\rho_i - \rho_k}{|i-k|^\mu} + \sum_{\substack{i \in \mathbb{Z} \\ 1 \le |i-k| \le L}}\frac{\rho_k}{|i-k|^\mu} = l^\mu \mathcal{L}(\rho_k) + z_L\rho_k \sim z_L\rho_k, \tag{17}$$

where we ignore the $O(l^\mu)$ term in the final step. Then by (17) and (16), we obtain

$$\begin{aligned}
\frac{\rho_k(t + \delta t) - \rho_k(t)}{\delta t} &= \frac{A_k}{\delta t}\sum_{1 \le |i-k| \le L}\left[\frac{\rho_i}{A_i}\frac{1}{z_l|i-k|^\mu} - \delta t\frac{\rho_i}{|i-k|^\mu z_L} - \frac{\rho_k}{A_k}\frac{1}{z_L|i-k|^\mu}\right] \\
&\quad - \frac{A_k}{\delta t}\sum_{1 \le |i-k| \le L}\left[\frac{\rho_i}{|i-k|^\mu}\frac{\mathcal{L}(A_i)l^\mu}{A_i^2 z_L^2} - \frac{\rho_i \mathcal{L} A_i}{A_i z_L^2|i-k|^\mu}l^\mu\delta t\right] + \Gamma \\
&\sim \frac{A_k}{\delta t}\sum_{1 \le |i-k| \le L}\left[\frac{\frac{\rho_i}{A_i} - \frac{\rho_k}{A_k}}{|i-k|^\mu z_L} - \frac{\rho_i}{|i-k|^\mu}\frac{\mathcal{L}(A_i)l^\mu}{A_i^2 z_L^2} - \delta t\frac{\rho_i}{|i-k|^\mu z_L}\right] + \Gamma \\
&\sim \frac{l^\mu}{z_L\delta t}\left[A_k\mathcal{L}\left(\frac{\rho_k}{A_k}\right) - \frac{\rho_k\mathcal{L}(A_k)}{A_k}\right] - A_k\rho_k + \Gamma,
\end{aligned} \tag{18}$$

where, at the second step, we ignore the $O(l^\mu\delta t)$ terms in the summation. We also observe that

$$\mathcal{L}(A_k) = \sum_{\substack{j \in \mathbb{Z} \\ 1 \le |j-k| \le L}}\frac{A_j - A_k}{(|j-k|l)^\mu} = \frac{1}{l}\sum_{\substack{j \in \mathbb{Z} \\ 1 \le |j-k| \le L}}\frac{A_j - A_k}{(|j-k|l)^\mu}l. \tag{19}$$

We make the following changes of variable

$$x = kl, y_j = jl, A_j = A(y_j), A_k = A(x).$$

Then the right hand side of (19) can be regarded as a midpoint Riemann sum on the interval defined as follows:

$$I := \left[x - (L + \frac{1}{2})l, x - \frac{1}{2}l\right] \cup \left[x + \frac{1}{2}l, x + (L + \frac{1}{2})l\right]. \tag{20}$$

7

Hence, (19) implies

$$\mathcal{L}(A_k) \sim \frac{1}{l} \int_M \frac{A(y) - A(x)}{|y - x|^\mu} dy, \tag{21}$$

$$\frac{l^\mu}{z_L \delta t} \mathcal{L}(A_k) = \frac{l^{\mu-1}}{z_L \delta t} \int_M \frac{A(y) - A(x)}{|y - x|^\mu} dy.$$

As l converges to 0, the integration is local at x, and we can apply Taylor expansion at x on the integrand to obtain

$$\begin{aligned}
\frac{l^\mu}{z_L \delta t} \mathcal{L}(A_k) &= \frac{l^{\mu-1}}{z_L \delta t} \int_M |y - x|^{-\mu} \left[A_x(x)(y - x) + A_{xx}(x) \frac{(y-x)^2}{2} + O((y-x)^3) \right] dy \\
&\sim \frac{l^{\mu-1}}{z_L \delta t} \left[\int_M \frac{A_x(x)(y-x)}{|y-x|^\mu} dy + \int_M \frac{A_{xx}(x)(y-x)^2}{2|y-x|^\mu} dy \right] \\
&= \frac{l^{\mu-1}}{z_L \delta t} \int_{x+\frac{1}{2}l}^{x+(L+\frac{1}{2})l} |y - x|^{2-\mu} A_{xx}(x) dy \\
&= \frac{l^2}{z_L \delta t (3 - \mu)} \left[(L + \frac{1}{2})^{3-\mu} - (\frac{1}{2})^{3-\mu} \right] A_{xx}(x),
\end{aligned} \tag{22}$$

where, at the second step, we ignore the $O((y-x)^{3-\mu})$ terms, since $|y - x| \ll 1$ and $\mu < 3$. Applying (22) to (18), we obtain

$$\rho_t = \frac{l^2}{\delta t z_L (3 - \mu)} \left[(L + \frac{1}{2})^{3-\mu} - (\frac{1}{2})^{3-\mu} \right] \left[A(\frac{\rho}{A})_{xx} - \frac{\rho}{A} A_{xx} \right] - A\rho + \Gamma. \tag{23}$$

To simplify the expressions, we reparametrize (23) as follows:

$$A = \bar{A}\omega, \rho = \frac{\bar{\rho}\omega}{\theta}, t = \frac{\bar{t}}{\omega}, \bar{\eta} = \frac{l^2 \eta}{2\delta t \omega}.$$

This together with (10) and (23) implies (we drop the bars for now)

$$A_t = \eta A_{xx} - A + \alpha + A\rho, \tag{24}$$

$$\rho_t = D \left[A(\frac{\rho}{A})_{xx} - \frac{\rho}{A} A_{xx} \right] - A\rho + \beta, \tag{25}$$

where

$$D = \frac{l^2}{\omega \delta t z_L (3 - \mu)} \left[(L + \frac{1}{2})^{3-\mu} - (\frac{1}{2})^{3-\mu} \right], \quad \alpha = \frac{A^0}{\omega}, \quad \beta = \frac{\Gamma\theta}{\omega^2}. \tag{26}$$

2.4   Numerical Simulations

To verify the derivation of the continuum limit, we compare the solutions of the discrete model (5) and (9), and the continuum limit (24) and (25) numerically. For the discrete model, we use the grid points x_i, $i = 1, 2, \cdots, 60$ with $x_i - x_{i-1} = 1/60$. For the continuum system we consider the computational domain $x \in [0, 1]$ with $\Delta x = 1/60$, $\Delta t = 1/3600$. We use forward Euler method for time discretizations and spectral method for space derivatives. Periodic boundary conditions are implemented in both cases.

For the sake of computation for the continuum limit, we assume periodic boundary conditions for the solution. Therefore, we also apply the periodic boundary condition to the discrete model.
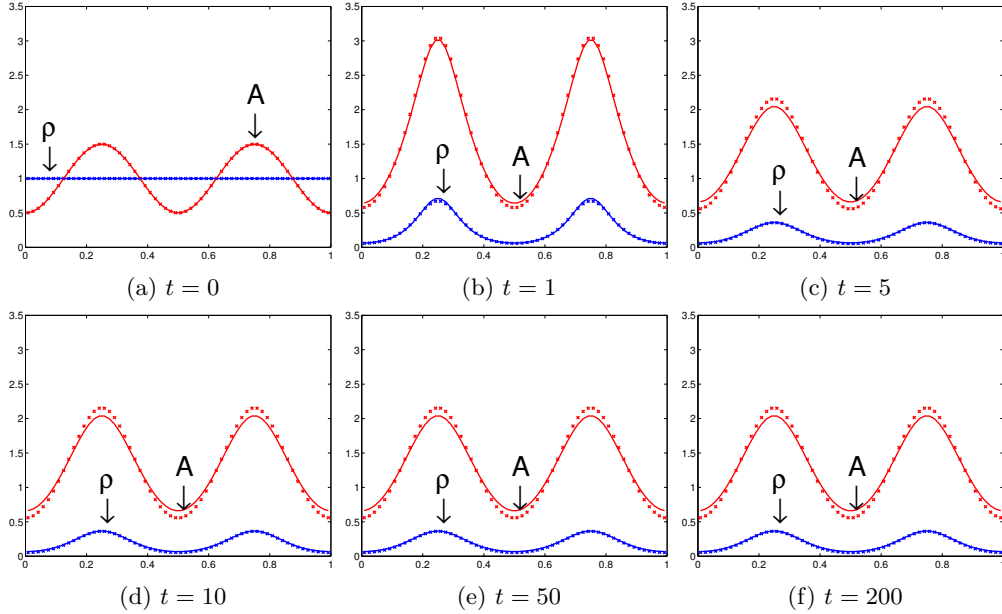
Figure 1: Simulations of biased truncated Lévy flight when $\mu = 2.5$, $l = 1/60$, $\delta t = 0.01$, and the speed limit L is 9. The solid curve represents the continuum limit, and the dots represent the discrete model. The initial conditions are taken to be $A^0 = 1 - 0.5\cos(4\pi x)$ and $\rho = 1$. Other relevant parameters are: $\eta = 0.1$, $\Gamma = 0.3$, $\omega = 1$

Figure 1 shows a comparison between our numerical simulations for the discrete and continuum models. We can observe a great agreement even at the boundary. However, periodic boundary condition is not so realistic (incorporating more realistic boundary conditions for the continuum model is discussed in [24]). Eventually, we observe a steady state with two hotspots for both models when time gets large.

Figure 2 compares the steady states of our models when the speed limit L is set to be distinct values, and Figure 3 compares the steady states for different values of μ. We see that the models fit one another fairly well for a large range of L and μ, providing numerical validity for our continuum model.

2.5   Linear Stability Analysis

To analyze the long-term behavior of the model, we perform a linear Turing stability analysis on (24) and (25) around the homogeneous steady state

$$\bar{A} = \alpha + \beta, \qquad \bar{\rho} = \frac{\beta}{\alpha + \beta}. \tag{27}$$

We perturb the steady state as follows

$$A(x,t) = \bar{A} + \delta_A e^{\lambda t} e^{ikx}, \qquad \rho(x,t) = \bar{\rho} + \delta_\rho e^{\lambda t} e^{ikx}. \tag{28}$$

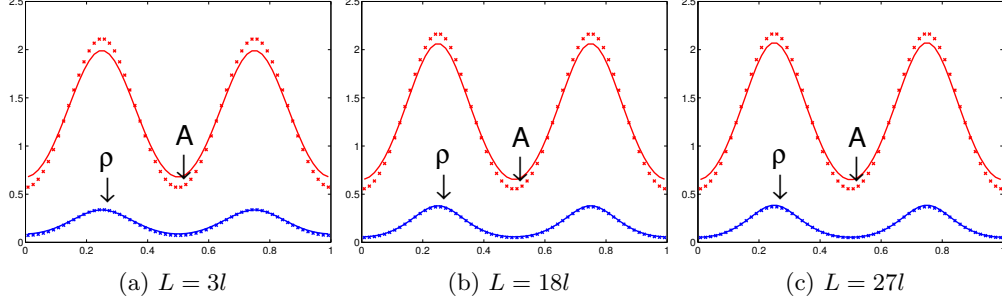9

(a) $L = 3l$ (b) $L = 18l$ (c) $L = 27l$

Figure 2: Comparisons of the steady state obtained using different L. All parameters are the same as in Figure 1 except L. The shots are taken at $t = 200$.
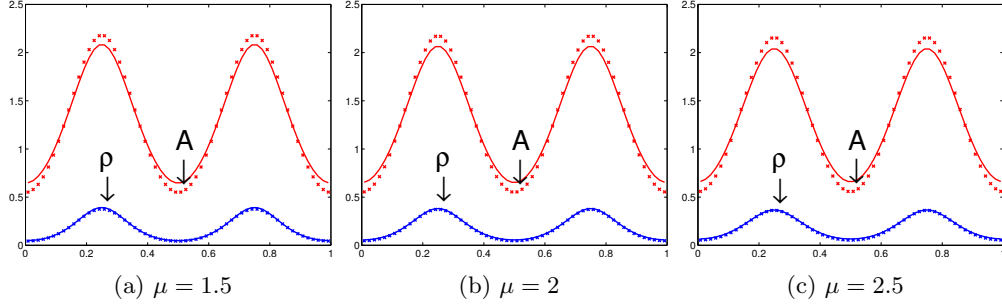

(a) $\mu = 1.5$ (b) $\mu = 2$ (c) $\mu = 2.5$

Figure 3: Comparisons of the steady state obtained using different μ. All parameters are the same as in Figure 1 except μ. The shots are taken at $t = 200$.

Substituting (28) into (24) and (25), we obtain

$$
\begin{bmatrix} -\eta|k|^2 - 1 + \bar{\rho} & \bar{A} \\ \frac{2\bar{\rho}}{\bar{A}}D|k|^2 - \bar{\rho} & -D|k|^2 - \bar{A} \end{bmatrix} \begin{bmatrix} \delta_A \\ \delta_\rho \end{bmatrix} = \sigma \begin{bmatrix} \delta_A \\ \delta_\rho \end{bmatrix} \tag{29}
$$

A detailed derivation of (29) can be found in the appendix. Furthermore, by analyzing (29), we obtain the following theorem characterizing the necessary and sufficient condition for the system to be unstable around the homogeneous steady state.

Theorem 2.1. *When $\bar{\rho} < 1/3$, the homogeneous equilibrium in (27) is stable. When $\bar{\rho} > 1/3$, then the equilibrium is unstable if and only if $\bar{A} < \bar{A}_*$, where*

$$
\bar{A}_* = D\eta^{-1}(\sqrt{3\bar{\rho}} - 1)^2. \tag{30}
$$

A proof of Theorem 2.1 can be found in the appendix.

2.6 Comparison with Previous Models

Now we compare the Truncated Lévy Flight Model with the Random Walk Model and the Lévy Flight Model. The equations for the attractiveness field are the same for all three models, and all the differences lie in the equations for the density of criminals.

10

2.6.1 Comparison with the Random Walk Model

We recall that the continuum limit in [19] for the criminal density in the one-dimensional Random Walk Model is as follows:

$$\rho_t = D_1 \left[A(\frac{\rho}{A})_{xx} - \frac{\rho}{A} A_{xx} \right] - A\rho + \beta, \tag{31}$$

where

$$D_1 = \frac{l^2}{2\omega\delta t}. \tag{32}$$

Comparing (25) and (31), we observe that they are the same except that D does not equal D_1. On the one hand, when L is large, the difference is prominent as is shown in figure 4. On the other hand, when $L = 1$, i.e., the criminals can move at most one grid in a single time step, which is exactly the same as the discrete Random Walk Model. Then we see that the solutions to (31) is close to the solutions to (25). Indeed, we have that $D \approx D_1$ when $L = 1$ and $\mu \in (1, 3)$ as shown in Figure 4. Thus, we can consider the Random Walk Model as a special case of our truncated Lévy flight when $L = 1$.
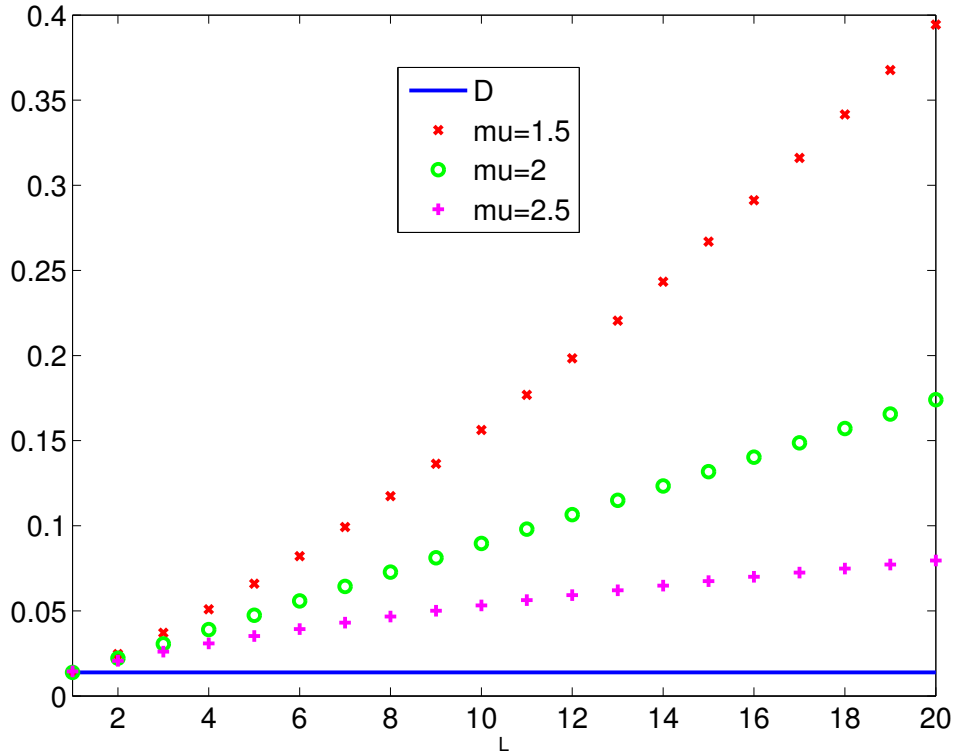

Figure 4: Comparisons of D (26) and D_1 (32) as a function of L with different μ's. The related coefficients are those in Figure 1.

11

2.6.2 Comparison with the Lévy Flight Model

The continuum limit in [4] for the criminal density in the one-dimensional Lévy Flight Model is

$$\rho_t = D_2 \left[A\Delta^s \frac{\rho}{A} - \frac{\rho}{A}\Delta^s A \right] - A\rho + \beta, \tag{33}$$

where

$$D_2 = \frac{l^{2s}}{\delta t} \frac{\pi^{1/2} 2^{-2s} |\Gamma(-s)|}{z\Gamma(s + \frac{1}{2})\omega}, \quad s = \frac{\mu - 1}{2}, \quad z = 2\sum_{n=1}^{\infty} \frac{1}{n^\mu}.$$

Notice that we have the fractional Laplace operator in (33), which is non-local. However, when L gets larger, the solution of the continuum truncated Lévy flight is closer to the solution of the continuum Lévy Flight Model, as is shown in figure 5.

2.6.3 Comparing the Solutions of the Three Models

As shown in Figure 5, the dynamics of the criminals in the Random Walk Model, Lévy Flight Model, and Truncated Lévy Flight Model are significantly different with identical initial conditions when $\mu = 2.5$ and $L \neq 1$. In LFM and TLFM, the criminals are more concentrated around the hotspots than in RWM, probably because the longer jumps in the Lévy flight allow criminals to aggregate on a hotspot more quickly. Moreover, LFM has more concentrated hotspots than the TLFM. Also, as mentioned above, we notice that when $L = 1$, the solution of TLFM behaves the same as the solution of RWM. However, as L increases to infinity, the truncated Lévy flight behaves more like a untruncated Lévy flight.

3 Modeling the Effects of Police Patrol

3.1 Criminological Background

The Random Walk Model has been generalized to model the effects of police activity as in [11]. Here, we will extend our truncated Lévy Flight Model to incorporate the effects of the law enforcement. Let $\psi_k(t)$ denote the number of officers at site k time t. As in [11], we introduce a new variable representing the attractiveness in the presence of police officers:

$$\tilde{A}_k(t) := e^{-\chi \psi_k(t)} A_k(t),$$

where χ is a given constant measuring police efficiency. In the discrete model, the relative weight of a criminal moving from i to k becomes

$$w_{i \to k} = \begin{cases} \frac{\tilde{A}_s}{l^\mu |i-k|^\mu}, & 1 \leq |i - k| \leq L, \\ 0, & \text{otherwise.} \end{cases} \tag{34}$$

Thus, the movement of criminals now obeys the following rule:

$$\rho_k(t + \delta t) = \sum_{1 \leq |i-k| \leq L} \rho_i (1 - \tilde{A}_i \delta t) q_{i \to k} + \Gamma \delta t. \tag{35}$$

The evolution of $B_k(t)$ becomes

$$B_k(t + \delta t) = \left[(1 - \eta) B_k(t) + \frac{\eta}{2}(B_{k-1} + B_{k+1}) \right] (1 - \omega \delta t) + \delta t \tilde{A}_k \rho_k \theta. \tag{36}$$
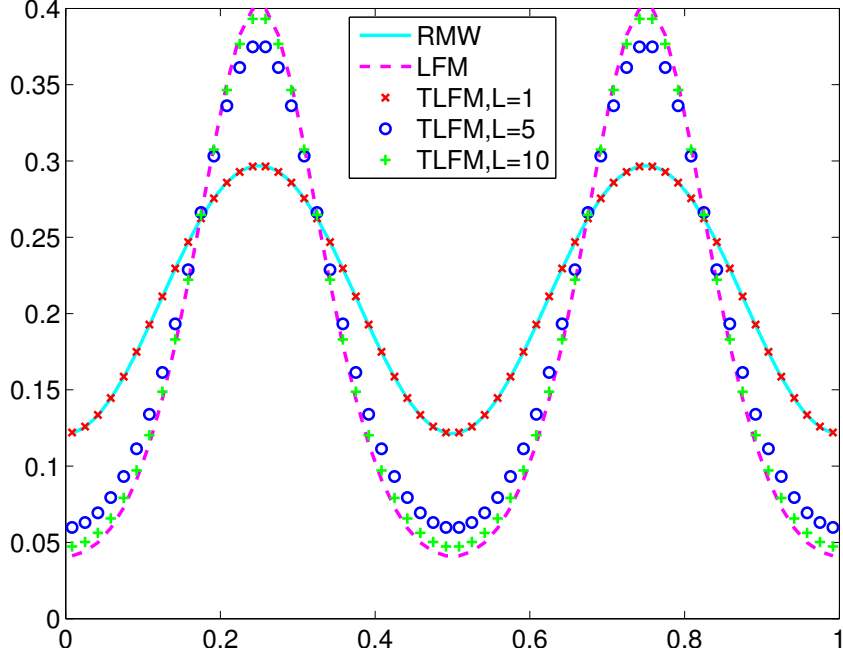
12

Figure 5: Comparing solutions of the Truncated Lévy Flight Model (with speed limit $L = 1, 5$, and 10), the Random Walk Model, and the Lévy Flight Model of the criminals when $t = 10$. The parameters and initial conditions are the same as in Figure 1.

Now the continuum limit for the evolution of A and ρ becomes

$$A_t = \eta A_{xx} - A + \alpha + \tilde{A}\rho, \tag{37}$$

$$\rho_t = D\left[\tilde{A}(\frac{\rho}{\tilde{A}})_{xx} - \frac{\rho}{\tilde{A}}\tilde{A}_{xx}\right] - \tilde{A}\rho + \beta. \tag{38}$$

Notice that in this model, the patrolling officers never arrest criminals, in accordance with the setting in [11]. Instead, the officers decrease the total number of burglary events by affecting the environment, that is, affecting $\tilde{A}$. We will discuss this effect in detail in the next section.

3.2 Dynamics of the Police

We assume that the total number of police officers is constant. This assumption reflects the reality that police departments have limited resources. Here we discuss the one dimensional case. We will propose a few applicable strategies for the police and compare the effectiveness of these strategies.

3.2.1 Random Walk

An unbiased random walk is perhaps the simplest strategy to implement. In each step, a police officer either moves one step to the left or to the right with equal probability. Thus,

13

the evolution of the number of officers satisfies the following relation:

$$\psi_k(t + \delta t) = \frac{1}{2}(\psi_{k-1}(t) + \psi_{k+1}(t)). \tag{39}$$

The continuum limit as l and δt both converge to 0 for the above equation is then as follows

$$\psi_t = \frac{l^2}{2\delta t}\psi_{xx}, \tag{40}$$

which is exactly the master equation for a standard Brownian motion. An obvious disadvantage of random walk is then clear: the spacial distribution of police will become nearly uniform in the long run. In other words, random walk does not give enough protection to important locations.

Figure 6 shows the effect of the unbiased random walk. We observe that random walking police reduce average site attractiveness. They do not however reduce hotspot activity.

This is consistent with the empirical evidence in [11]. Therefore, we will treat the random walk strategy as a "control group", and introduce two more effective strategies.
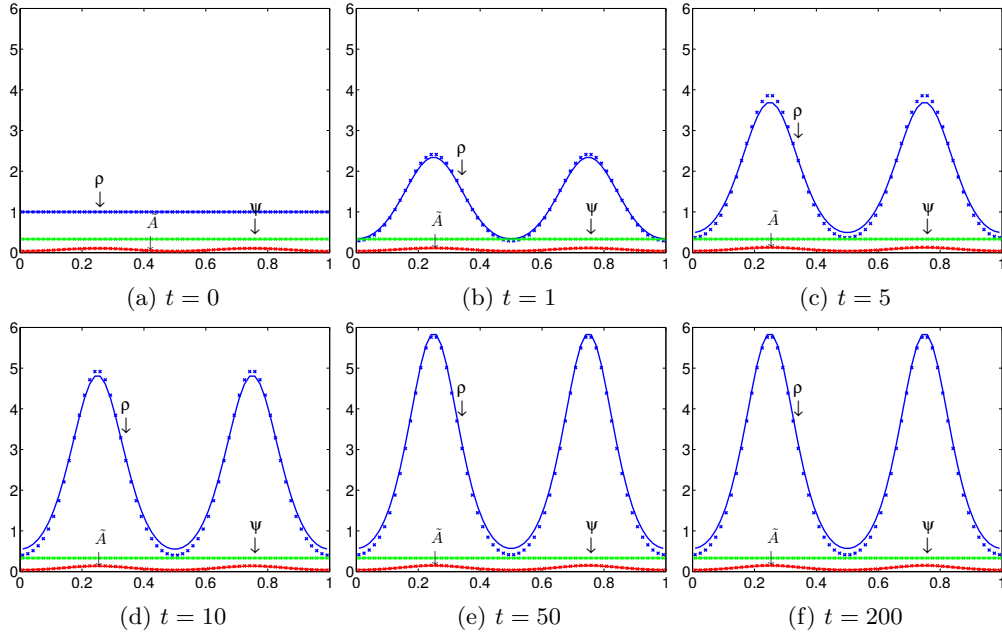

Figure 6: The comparison of the discrete model and its continuum limit when the criminals follow a truncated Lévy flight and the police follow an unbiased random walk. The green curve and dots represent officers in the continuum and discrete model respectively. The parameters for the criminal are the same as in Figure 1. The initial conditions for the police are $\psi = 1/3$. Also we set $\chi = 8$

3.2.2 Biased Random Walk

We hope that the police can be attracted to criminal hotspots, so we make the strategy of the police biased towards the same attractiveness as criminals. Then the discrete evolution

equation for the police adopting a random walk biased towards the hotspots can be written as

$$\psi_k(t + \delta t) = \frac{A_k}{A_k + A_{k-2}} \psi_{k-1}(t) + \frac{A_k}{A_k + A_{k+2}} \psi_{k+1}(t). \tag{41}$$

The corresponding continuum limit is then

$$\psi_t = \frac{l^2}{2\delta t} \left[A(\frac{\psi}{A})_{xx} - \frac{\psi}{A} A_{xx} \right]. \tag{42}$$

This strategy is also studied in [23], and is referred to as "cops on the dots".

The effect of this strategy is shown in Figure 7. We observe that the long-term distribution of the police officers generally corresponds to that of the attractiveness. Also, the average value of ρ is lower and approaches a steady state faster than in the case when police follow an unbiased random walk.
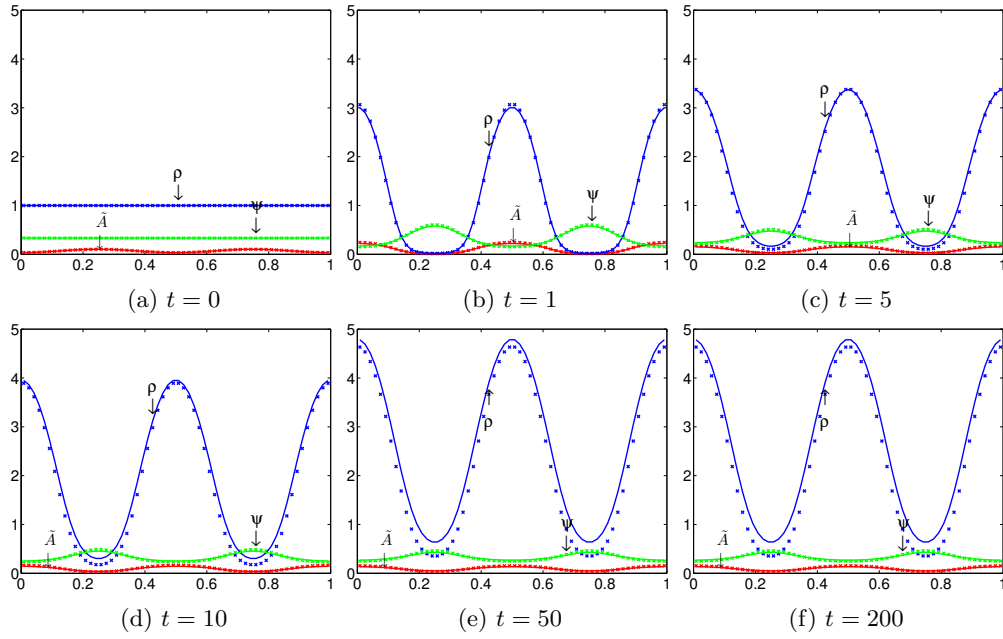

Figure 7: The comparison of the discrete model and its continuum limit when the criminals follow a truncated Lévy flight and the police follow a biased random walk. The parameters are the same as in Figure 6.

3.2.3 Biased Truncated Lévy Flight

As we have discussed in the introduction, a truncated Lévy flight reasonably approximates the dynamics of the criminals. The police, naturally, can also choose a truncated Lévy flight as a patrol strategy. The discrete dynamics of the police taking a biased truncated Lévy flight is as follows

$$\psi_k(t + \delta t) = \sum_{|i-k| \leq L} \psi_i(t) q_{i \to k}(t), \tag{43}$$

where

$$q_{i \to k} = \frac{w_{i \to k}}{\sum_j w_{i \to j}}, \tag{44}$$

and

$$w_{i \to k} = \begin{cases} \frac{A_k}{l^\mu |i-k|^\mu}, & 1 \le |i-k| \le L, \\ 0, & \text{otherwise.} \end{cases} \tag{45}$$

We set the patrolling strategy of the police to have the attractiveness field A_k so that they are biased towards the crime hotspots. Also, the police and the criminals share the same parameters μ and L in the underlying Lévy power law, reflecting the reality that all modes of transport available to criminals are also available to police. Moreover, this strategy is easy to deploy, since the police only need to move up to L steps in δt.

We derive the continuum limit for this case in the same way as in Section 2.3, and obtain

$$\psi_t = D \left[A \left(\frac{\psi}{A} \right)_{xx} - \frac{\psi}{A} A_{xx} \right]. \tag{46}$$

We note that the above continuum limit does not have the linear terms, $-A\rho + \beta$, as in (25), because the number of police officers should be conserved.

We simulate this case in Figure 8. Comparing Figure 8 and Figure 7, we see that there is not much qualitative difference between the two steady states. To address the difference between the two strategies, we will examine the quantitative difference of the total number of crimes in a given time period closely in the next subsection.
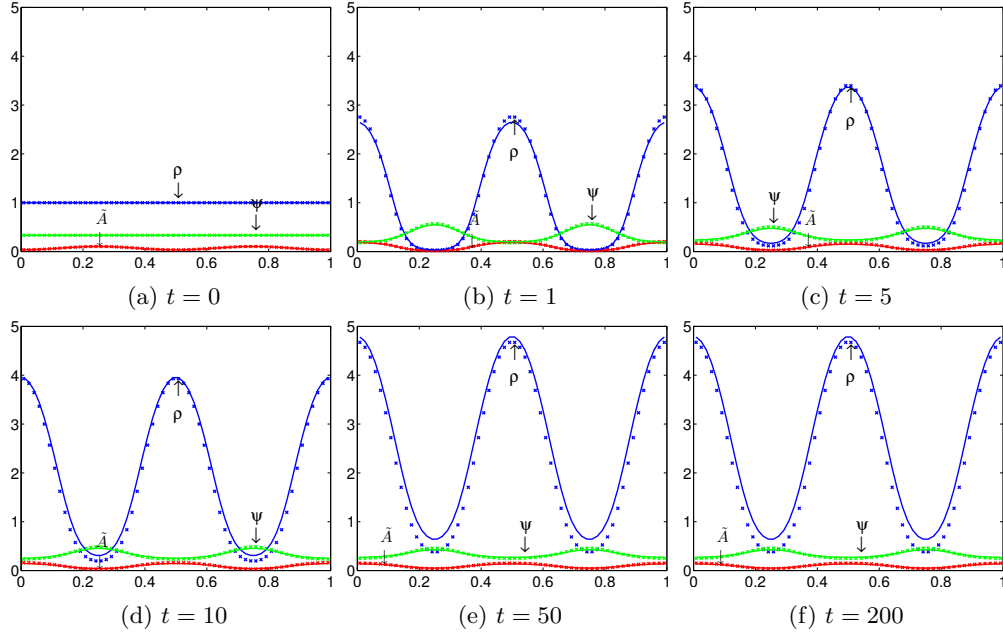

Figure 8: The comparison of the discrete model and its continuum limit when the criminals follow a truncated Lévy flight and the police also follow a biased truncated Lévy flight. The parameters are the same as in Figure 6.

3.3 Evaluation of Different Patrol Strategies

In this section, we will evaluate the effectiveness of each patrolling strategy quantitatively. The expectation of total number of burglary events, which we denote as S, is naturally a good measure of the effectiveness. Recall that $E_k(t)$, the number of burglary events at location k in the time interval $(t, t+\delta t)$, has expectation $\tilde{A}_k(t)\rho_k(t)\delta t$. Then the total number of burglary events until time T has expectation $\sum_k \sum_{t<T} \tilde{A}_k(t)\rho_k(t)\delta t$. When we take the continuum limit as t and l converge to 0, the previous double sum is approximated by a double integral, which we define as S:

$$S(T) = \int_0^T \int_{\mathcal{M}} \tilde{A}(x,t)\rho(x,t)dxdt, \tag{47}$$

where $\mathcal{M}$ is our spacial domain. In practice, the domain $\mathcal{M}$ is bounded, thus has a finite measure. Furthermore, we define the instantaneous crime rate $R(t)$ at time t as

$$R(t) := \frac{\partial S}{\partial t}(t) = \int_{\mathcal{M}} \tilde{A}(x,t)\rho(x,t)dx. \tag{48}$$

Police Pattern	S(5)	Improvement 1	Improvement 2
No Police	13874	-	-
Random Walk	9316.6	32.85%	-
Biased Random Walk	9124.6	34.23%	2.06%
Biased Truncated Lévy Flight	8750.0	36.93%	18.16%

Table 1: The expectation of total number of burglary events S before time $T = 5$ when the cops follow different patterns using the parameters and initial conditions in Figure 5. Improvement 1 shows the corresponding improvement compares to the situation without cops, and improvement 2 compares to situation when cops choose unbiased random walk. The initial condition in this case simulates the situation that there are two major regions of high attractiveness to the criminals.

Police Pattern	S(5)	Improvement 1	Improvement 2
No Police	13827	-	-
Random Walk	9890.1	28.47%	-
Biased Random Walk	9269.0	32.96%	6.28%
Biased Truncated Lévy Flight	8836.8.0	36.09%	10.65%

Table 2: The expectation of total number of burglary events S before time $T = 5$ when the cops follow different patterns with the same parameters and initial conditions as in Table 1, except that $A^0 = 1 - 0.5\cos(8\pi x)$, and $\rho = 1 - 0.3\cos(8\pi x)$. In this case, there are initially four regions of high attractiveness. We observe that the biased truncated Lévy flight is still the best strategy among the three.
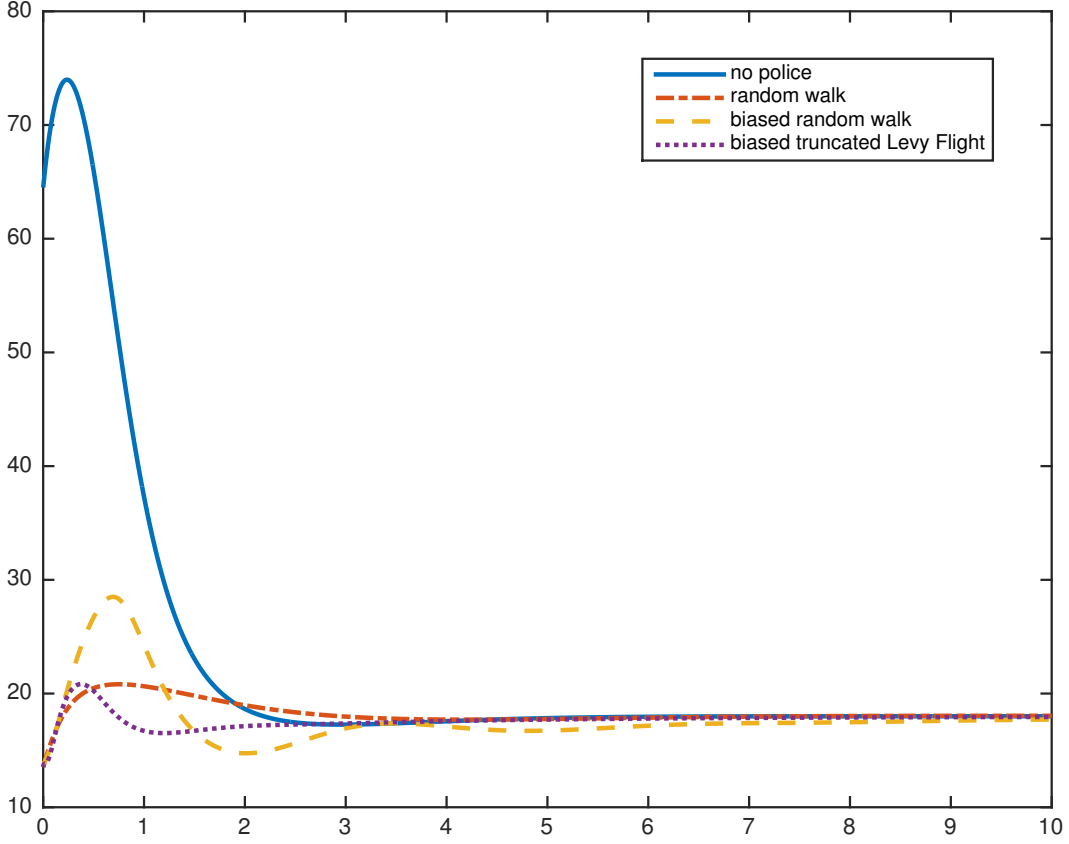
Figure 9: The plot of $R(t)$. The initial conditions are $A^0 = 1 - 0.5\cos(4\pi x)$, $\rho = 1 - 0.3\cos(4\pi x)$, and $\psi = 1/3\sin(\pi x)$.

3.3.1 Steady State Crime Rate

We observe that, the crime rate in our model, regardless of hotspot activity, will approach a constant which equals to the rate of criminals entering the system.

Theorem 3.1. *We assume periodic boundary conditions with (24) and (25) on the spacial domain $\mathcal{M}$. If (24) and (25) is in a steady state, then the crime rate within the system is equal to $\beta|\mathcal{M}|$, where $|\mathcal{M}|$ is the measure of $\mathcal{M}$.*

Proof. We integrate (38) over the domain $\mathcal{M}$, and obtain

$$\frac{\mathrm{d}}{\mathrm{d}t}\int_{\mathcal{M}}\rho = \int_{\mathcal{M}}\rho_t = \int_{\mathcal{M}} D\left[\tilde{A}\left(\frac{\rho}{\tilde{A}}\right)_{xx} - \frac{\rho}{\tilde{A}}\tilde{A}_{xx}\right] - \tilde{A}\rho + \beta dx$$
$$= \left[\tilde{A}(\frac{\rho}{\tilde{A}})_x - \frac{\rho}{\tilde{A}}\tilde{A}_x\right]\Big|_{\mathcal{M}} - \int_{\mathcal{M}}(\tilde{A}\rho - \beta)dx. \tag{49}$$

With periodic boundary conditions on $\mathcal{M}$, we have

$$\frac{\mathrm{d}}{\mathrm{d}t}\int_{\mathcal{M}}\rho = \beta|\mathcal{M}| - \int_{\mathcal{M}}\tilde{A}\rho = \beta|\mathcal{M}| - R. \tag{50}$$

18

Police Pattern	S(5)	Improvement 1	Improvement 2
No Police	13758	-	-
Random Walk	10006	27.27%	-
Biased Random Walk	9227.1	32.93%	7.78%
Biased Truncated Lévy Flight	8489.5	38.29%	15.16%

Table 3: The expectation of total number of burglary events S before time $T = 5$ when the cops follow different patterns using the same parameters and initial conditions as in Table 1, except that $A^0 = 1 - 0.5\cos(16\pi x)$, and $\rho = 1 - 0.3\cos(16\pi x)$, i.e. there are initially eight regions of high attractiveness, even more hotspots than before. We observe that the biased truncated Lévy flight is again the best strategy among the three.

When the system is at a steady state, we have

$$\frac{\mathrm{d}}{\mathrm{d}t}\int_{\mathcal{M}}\rho = 0.$$

It follows that

$$R(t) = \beta|\mathcal{M}|. \tag{51}$$

$\square$

This implies that the crime rate will eventually converge to a constant. As a result, we shall only focus on the effect of patrol before the crime rate getting close enough to this constant rate. Furthermore, we notice that when $T \geq 5$, with a set of chosen initial conditions and parameters, the crime rate is always within 5% difference compared with the steady state crime rate. In other words, significant difference of crime rates only arise within the time interval $T \in [0, 5)$. Therefore, we only need to compare $S(5)$ to measure the effects of different strategies. We find that, as shown in Table 1, 2 and 3, the police reduce the total number of crimes most effectively when they choose biased truncated Levy flight. We set certain cosine functions as the initial conditions for A^0, ρ and ψ in order to simulate different cases with different number of crime hotspots initially. We see that regardless of the number of hotspots initially, the biased truncated Lévy flight tends to outperform the biased random walk and the unbiased random walk.

3.4 Simulations in Two Dimension

To get a better understanding of how different strategies behave in the real life phenomena, we now show the discrete simulations in the two dimensional domain, that is, we extend the discrete models discussed in section 3.2 and 3.3 to the two dimensional case. We discretize the domain, and define the distance between two grid points as their Euclidean distance. Then, we create dynamics arrays cr_{pos} and pol_{pos} to store the locations of criminals and polices. In addition, we create arrays A, B, ψ to represent A, B, and the density of polices, and 2D arrays A_{2D}, B_{2D} to represent A and B in the 2D space. In addition, we use array E to represent the number of crimes committed at each spot at each time step. At each time step a specific person (a criminal or a police officer) will make his or her own decision based on our discrete formulation as described in (5), (9), (39), (41), and (43). The algorithm is outlined as follows

---

program **2D Simulation**

input n, Δt number of criminals N_c, number of the police N_p, initial attractiveness $A_0(x_i)$, and model parameters L, μ, η, ω, β, χ

for $t_k = 1 : (t/\delta t)$

    Initialize E to be 0.
    Calculate the probability of a criminal committing a crime at each spot.

    for $i = 1 : N_c$

        Determine whether the ith criminal will commit a crime based on its location and a random number we generate.

        If it commits a crime, update E.

        Otherwise, determine where it goes following a biased truncated Lévy flight.

        Update cr_{pos}.

    end

    for $i = 1 : N_p$

        Determine where the ith police will go based on the strategy of the police.

        Update pol_{pos}.

    end

    Update ψ based on pol_{pos}.

    Update A, B based on E and ψ.

end

end **2D Simulation**

(a) No Police

(b) Random Walk

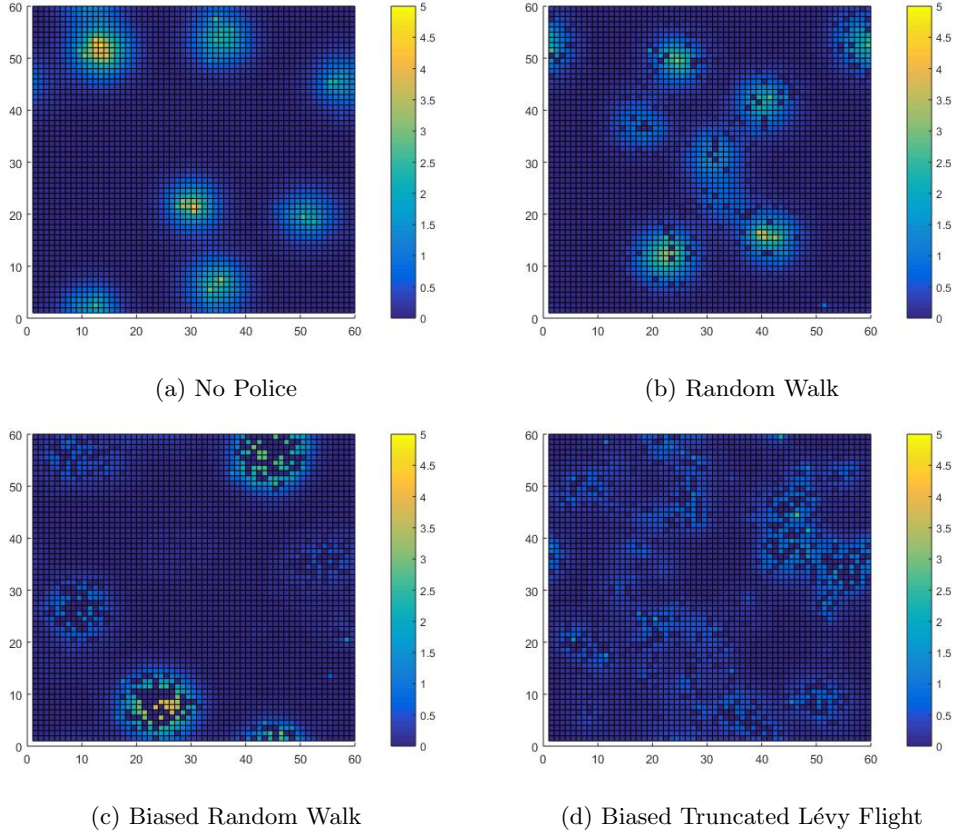(c) Biased Random Walk

(d) Biased Truncated Lévy Flight

Figure 10: The simulations in two dimension when the police follow different strategies as shown in (a)-(d). The color represents the attractiveness of certain spots. We set the main parameters to be $\mu = 2.5$, $l = 1/60$, $\delta t = 0.01$, and the speed limit is $L = 9$. Also, we let $\omega = 1/15$, $\theta = 1$, and $\eta = 0.03$. For the initial condition, we set $A^0 \equiv 1/30$ and 1000 criminals and 500 polices randomly distributed on the 3600 grids. We run the simulations for 1000 steps.

To simulate this stochastic process, we use the Monte Carlo method. Figure 10 shows the result of the simulations. We observe that the police reduce the attractiveness most effectively when they adopt the biased truncated Lévy flight. From this observation, we infer via equation (48) that the biased truncated Lévy flight reduces crime rate better than other strategies. Also, a biased random walk strategy is better than an unbiased random walk strategy. These results agree with the corresponding results in the one-dimension model.

4   Discussion

The Truncated Lévy Flight Model generalizes both the Random Walk Model and the Lévy Flight Model in the following sense. Firstly, the discrete biased random walk is a special case of the discrete biased truncated Lévy flight when $L = 1$. Meanwhile, the continuum

limit of RWM matches the continuum limit of TLFM. Secondly, as $L \to \infty$, the discrete truncated Lévy Flight Model approaches closely to the discrete Lévy Flight Model, while the solutions of the continuum truncated Lévy flight behaves similarly to the solutions of the continuum Lévy flight as in Figure 4.

We then consider the effects of police patrol assuming that the criminals follow a truncated Lévy flight. We select the three executable strategies: an unbiased random walk, a biased random walk, and a biased truncated Lévy flight. The results in Section 3.3 show that, with spatially non-uniform initial conditions, the most effective strategy among the three is the biased truncated Lévy flight. Although in this paper, we only focus on the three strategies mentioned above, we hope to find a better executable strategy for the police in the future.

As we have simulated the dynamics of police and criminals in a two-dimensional domain, a future work will be to generalize all our results to the two-dimensional case for the derivation of the continuum limit. Also, in order to further analyze the effect of police patrol, we hope to introduce a term to allow criminals leaving the system without committing a crime with the appearance of the police .

5 Appendix

We first show a detailed derivation for (29). Recall that in Section 2.5, we want to examine the behavior of solutions of the form

$$A(x,t) = \bar{A} + \delta_A e^{\sigma t} e^{ikx}, \tag{52}$$

$$\rho(x,t) = \bar{\rho} + \delta_\rho e^{\sigma t} e^{ikx}. \tag{53}$$

Substituting the solutions into (25), we obtain

$$-\eta|k|^2 \delta_A e^{\sigma t} e^{ikx} - \bar{A} + A_0 - \delta_A e^{\sigma t} e^{ikx} + (\bar{A} + \delta_A e^{\sigma t} e^{ikx})(\bar{\rho} + \delta_\rho e^{\sigma t} e^{ikx}) = \sigma \delta_A e^{\sigma t} e^{ikx},$$

$$-\eta|k|^2 \delta_A - \delta_A + \bar{\rho}\delta_A + \bar{A}\delta_\rho + \delta_A \delta_\rho e^{\sigma t} e^{ikx} = \sigma \delta_A. \tag{54}$$

We rewrite (54) in the matrix form, ignoring the second order term $\delta_A \delta_\rho e^{\sigma t} e^{ikx}$, and obtain

$$\begin{bmatrix} -\eta|k|^2 - 1 + \bar{\rho} & \bar{A} \end{bmatrix} \begin{bmatrix} \delta_A \\ \delta_\rho \end{bmatrix} = \sigma \delta_A \tag{55}$$

Similarly for ρ, from (53), we derive the the corresponding matrix equation as follows

$$\begin{bmatrix} -\frac{2\bar{\rho}}{\bar{A}} D|k|^2 - \bar{\rho} & -D|k|^2 - \bar{A} \end{bmatrix} \begin{bmatrix} \delta_A \\ \delta_\rho \end{bmatrix} = \sigma \delta_\rho \tag{56}$$

Combining (55) and (56), we thus obtain (29).

Now we provide a proof for Theorem 2.1.

Proof of Theorem 2.1. To solve the eigenvalue problem (29), we first rewrite (29) as

$$\begin{bmatrix} -\eta|k|^2 - 1 + \bar{\rho} - \sigma & \bar{A} \\ \frac{2\bar{\rho}}{\bar{A}} D|k|^2 - \bar{\rho} & -D|k|^2 - \bar{A} - \sigma \end{bmatrix} \begin{bmatrix} \delta_A \\ \delta_\rho \end{bmatrix} = 0 \tag{57}$$

22

By setting the determinant of the square matrix in the left hand side of (57) to be zero, we obtain

$$\sigma^2 - \tau\sigma + \delta = 0, \tag{58}$$

where

$$\tau = -D|k|^2 - \eta|k|^2 - \bar{A} - 1 + \bar{\rho}, \tag{59}$$

$$\delta = D|k|^2(\eta|k|^2 + 1 - 3\bar{\rho}) + \eta|k|^2\bar{A} + \bar{A}. \tag{60}$$

We know that the equilibrium is stable if and only if both solutions to (58) have negative real parts. Since $\alpha, \beta > 0$, and thus $\bar{A} > 0, 0 < \bar{\rho} < 1$, we observe that $\tau \leq 0$. Therefore, the equilibrium is stable if and only if $\delta > 0$. We then observe that if $\bar{\rho} < 1/3$, then $\delta > 0$. It follows that the equilibrium is stable when $\bar{\rho} < 1/3$.

Now we consider the case when $\bar{\rho} > 1/3$. Since the equilibrium is unstable if and only if $\delta < 0$, from (60) we rewrite the condition $\delta < 0$ equivalently as

$$\bar{A} < D|k|^2\left(-1 + \frac{3\bar{\rho}}{\eta|k|^2 + 1}\right), \forall k. \tag{61}$$

We set $x = \eta|k|^2$. From (61), we obtain

$$\bar{A} < \bar{A}_* = \max_{x \geq 0}[D\eta^{-1}x\left(-1 + \frac{3\bar{\rho}}{x+1}\right)]. \tag{62}$$

We then calculate the right-hand side of (62) by setting the derivative of the corresponding function equal to zero, and we obtain

$$D\eta^{-1}x\frac{-3\bar{\rho}}{(x+1)^2} + D\eta^{-1}(-1 + \frac{3\bar{\rho}}{x+1}) = 0,$$

$$x^2 + 2x + 1 - 3\bar{\rho} = 0. \tag{63}$$

The positive root of (63) is $x = -1 + \sqrt{3\bar{\rho}}$ (recall that $\bar{\rho} > \frac{1}{3}$), which we substitute into (62) and obtain

$$\bar{A} < \bar{A}_* = D\eta^{-1}(-1 + \sqrt{3\bar{\rho}})^2, \tag{64}$$

which serves as the stability condition as in (30).

To conclude, when $\bar{\rho} < 1/3$, the equilibrium is stable. When $\bar{\rho} > 1/3$, the equilibrium is unstable if and only if (64) is satisfied. $\qquad\square$

6   Acknowledgements

References

[1] A. L. Bertozzi, P. J. Brantingham, and G. Mohler, "Dynamic models of insurgent activity," DTIC Document, Tech. Rep., 2014.

[2] D. Brockmann, L. Hufnagel, and T. Geisel, "The scaling laws of human travel," *Nature*, vol. 439, January 2006.

[3] T. Budd, "Burglary of domestic dwellings: Findings from the british crime survey," *Home Office Statistical Bulletin 4/99*, vol. Home Office: London, 1999.

[4] S. Chaturapruek, J. Breslau, D. Yazdi, T. Kolokolnikov, and S. G. McCalla, "Crime modeling with Lévy flights," *SIAM J. Appl. Math.*, vol. 73, no. 4, pp. 1703–1720, 2013.

[5] K. J. Chechkin A V, Metzler R and G. V. Yu, "Introduction to the theory of Lévy flights," *International Journal of Theoretical and Applied Finance*, vol. 3, 2008.

[6] J. M. Gau and T. C. Pratt, "Revisiting broken windows theory: Examining the sources of the discriminant validity of perceived disorder and crime," *Journal of Criminal Justice*, vol. 38, no. 4, pp. 758 – 766, 2010.

[7] M. C. González, C. A. Hidalgo, and A.-L. Barabási, "Understanding individual human mobility patterns," *Nature*, vol. 453, June 2008.

[8] J. N. H. Berestycki, "Self-organised critical hot spots of criminal activity," *European Journal of Applied Mathematics*, vol. 21, October 2010.

[9] B. E. Harcourt, "Reflecting on the subject: A critique of the social influence conception of deterrence, the broken windows theory, and order-maintenance policing new york style," *Michigan Law Review*, vol. 97, no. 2, pp. 291–389, 1998.

[10] A. James, M. J. Plank, and A. M. Edwards, "Assessing lévy walks as models of animal foraging," *Journal of the Royal Society, Interface*, vol. 8, September 2011.

[11] P. A. Jones, P. J. Brantingham, and L. R. Chayes, "Statistical models of criminal behavior: the effects of law enforcement actions," *Math. Models Methods Appl. Sci.*, vol. 20, no. suppl. 1, pp. 1397–1423, 2010.

[12] P. J. V. Koppen, R. W. J. J. Short, P. J. Brantingham, A. L. Bertozzi, and G. E. Tita, "The road to the robbery: Travel patterns in commercial robberies," *Br. J. Criminol*, vol. 38, pp. 230–246, 1998.

[13] R. L.Cuoto Miranda, "Truncated Lévy walks and an emerging market economic index," *Physica A: Statistical Mechanics and its Applications*, vol. 297, pp. 509–520, August 2001.

[14] R. N. Mantegna and H. E. Stanley, "Stochastic process with ultraslow convergence to a gaussian: The truncated lévy flight," *Phys. Rev. Lett.*, vol. 73, pp. 2946–2949, Nov 1994.

[15] A. Matacz, "Financial modeling and option theory with the truncated levy process," *International Journal of Theoretical and Applied Finance*, vol. 3, no. 1, 2000.

[16] Y. L. M.C. Mariani, "Normalized truncated levy walks applied to the study of financial indices," *Physica A: Statistical Mechanics and its Applications*, vol. 377, pp. 590–598, April 2007.

[17] M. O'Leary, "Modeling criminal distance decay," *Cityscape: A Journal of Policy Development and Research*, vol. 13, 2011.

[18] M. Short, P. J. Brantingham, A. L. Bertozzi, and G. E. Tita, "Dissipation and displacement of hotspots in reaction-diffusion models of crime," *Proc. Nat. Acad. Sci.*, vol. 107, no. 9, pp. 3961–3965, 2010.

[19] M. B. Short, M. R. D'Orsogna, V. B. Pasour, G. E. Tita, P. J. Brantingham, A. L. Bertozzi, and L. B. Chayes, "A statistical model of criminal behavior," *Math. Models Methods Appl. Sci.*, vol. 18, no. suppl., pp. 1249–1267, 2008.

[20] M. B. Short, A. L. Bertozzi, and P. J. Brantingham, "Nonlinear patterns in urban crime: Hotspots, bifurcations, and suppression," *SIAM Journal on Applied Dynamical Systems*, vol. 9, no. 2, pp. 462–483, 2010.

[21] B. Snook, "Individual differences in distance travelled by serial burglars," *Journal of Investigative Psychology and Offender Profiling*, vol. 1, 2004.

[22] D. L. Weisel, R. V. Clarke, and J. R. Stedman, "Hot dots in hot spots: Examining repeat victimization for residential burglary in three cities, final report," 1999.

[23] J. R. Zipkin, M. B. Short, and A. L. Bertozzi, "Cops on the dots in a mathematical model of urban crime and police response," *Discrete Contin. Dyn. Syst. Ser. B*, vol. 19, no. 5, pp. 1479–1506, 2014.

[24] A. Zoia, A. Rosso, and M. Kardar, "Fractional laplacian in bounded domains," *Physical Review*, vol. 76, no. 4, 2007.